INTERNATIONAL JOURNAL FOR NUMERICAL METHODS IN FLUIDS, VOL. 20, 1337–1361 (1995)

ADVECTION OF AXISYMMETRIC INTERFACES BY THE VOLUME-OF-FLUID METHOD

F. MASHAYEK AND N. ASHGRIZ

Department of Mechanical and Aerospace Engineering, State University of New York at Buffalo, Buffalo, NY 14260, U.S.A.

SUMMARY

A criterion is proposed for the advection of axisymmetric interfaces. The location of an interface is followed by a volume-tracking technique wherein a volume fraction parameter is assigned to each of the cells in a Eulerian grid system. The interface is discretized into a set of line segments fitted at the boundary of every pair of neighbouring computational cells. The orientation of a line segment is obtained by inspecting the volume fractions of two neighbouring cells. The volume fractions are then advected using the velocity components at the boundary of the two cells. The following advection criterion is proposed: for advection in the axial direction the axial velocity u is assumed constant in the vicinity of each cell face; for advection in the radial direction the radial velocity v times the radial distance r is assumed constant in the vicinity of each cell face, i.e. $r^{\beta}v = \text{const.}$, where $\beta = 0$ for Cartesian and $\beta = 1$ for axisymmetric systems. The above criterion is used to develop an algorithm for the advection of axisymmetric interfaces which is referred to as the 'axisymmetric flux line segment model for advection and interface reconstruction' or A-FLAIR.

KEY WORDS: volume-of-fluid; surface reconstruction; interface advection

1. INTRODUCTION

There are numerous physical phenomena and industrial processes in which two immiscible fluids or materials having different phases are in direct contact with each other. The numerical simulation of the complex topology of the interfaces between these fluids and different material phases has been one of the most challenging problems in computational fluid dynamics. Numerical modelling of these flows is complicated by the difficulty in describing the transient and irregular interface boundary conditions. Various techniques have been developed and their accuracy has been determined by the extent to which the physics of the interface is predicted. Reviews of different techniques for flows with interfaces have been provided by Hyman,[1] Lasky *et al.*[2] and Floryan and Rasmussen.[3]

One of the techniques for simulating the interfaces is based on tracking the volume of each of the fluid components in the system. Upon discretization of the fluids into fixed Eulerian grid cells, a parameter is defined which represents the fraction of a cell volume occupied by one of the fluids. For a particular cell, if this fraction is zero or unity, the cell is either empty or full of that fluid respectively. Therefore the cell does not contain an interface between this fluid and other fluids in the system. However, if the volume fraction is between zero and unity, then the cell is an interface cell and has to be treated in a special manner. Similarly, a volume fraction parameter can be defined for other fluids in the system. The difficulty in using the cell volume fraction parameter to track the interface lies in (i) accurately advecting this quantity across the cell boundaries and (ii) reconstructing the interface based on the new advected volume fractions. Different techniques have been developed to handle each of these problems.

CCC 0271–2091/95/121337–25

Received 9 September 1993
Revised 25 August 1994

One of the earliest works in this direction was by DeBar.[4] In his paper DeBar described the fundamentals of the KRAKEN code, which is a Eulerian hydrodynamic code capable of locating fluid interfaces in the compressible inviscid flow of several fluids in a two-dimensional region. A sloped line segment was used to describe the interface. Advection of the interface was achieved by using local velocities to move the intersection points of the interface line with the cell boundaries. This resulted in a stretching of the interface and therefore violated conservation of mass at each advection. The latter problem was eliminated by specifying limitations on the allowable height of fluid in the cell.

Noh and Woodward[5] developed the simple line interface calculation (SLIC) algorithm in which the interface in each cell is assumed to be oriented either vertically or horizontally (i.e. parallel to the Eulerian co-ordinate axes). The interface line position in the cell is then easily obtained by simply knowing the fluid volume fraction. In addition, the assumption is made that the fluid resides on the side of the interface line where the neighbouring cells are mostly filled with the same fluid. The interface is then advected in the vertical and horizontal directions. Clearly, limiting the interface orientation to being either vertical or horizontal introduces the possibility of generating significant errors.

Subsequently, Chorin[6,7] improved the SLIC method with regard to both interface shape and its advection by adding a corner interface to the horizontal and vertical lines. He also allowed advection of the interface in the diagonal directions. Hence, instead of just the four possible advection directions in SLIC, eight directions became possible. Huygen's principle was then used to determine the direction of the interface advection. This technique was used by Ghoniem *et al.*[8,9] and Sethian[10] to study flame propagation in premixed gases and by Colella *et al.*,[11] Henderson *et al.*,[12] and Puckett[13] to study shock wave refraction.

Hirt and Nichols,[14] and Nichols *et al.*[15] introduced the volume-of-fluid (VOF) method, another improvement to the SLIC algorithm. They determined the direction of the interface by inspecting the volume fractions in the 3×3 block of neighbouring cells. However, for the advection they used the donor–acceptor flux approximation of Ramshaw and Trapp[16] in conjunction with the vertical and horizontal interfaces originally assumed in SLIC. Several other donor-based methods have been developed, one of the more recent ones being the partial donor cell method (PDM) of Hain.[17] PDM combines a second-order scheme with a donor cell method in such a way as to minimize diffusion and assure monotonicity. Barr and Ashurst[18] combined VOF and Chorin's version of SLIC to produce a method called SLIC–VOF. They showed that using this technique to advect curved interfaces results in a flattening or even an indentation of the interface.

Youngs[19] modified the VOF method to calculate the interface slope in each cell. The slope of the interface in a cell and the location of the fluid were obtained by inspecting the volume fractions in the eight neighbouring cells. The position of the interface in the cell is adjusted to match the volume fraction of the fluid under consideration. However, the interface reconstructed by this technique is not continuous, since the intersection point of the interface with the cell face is different in two neighbouring cells. Marcus *et al.*[20] and Henderson *et al.*[21] used the least squares technique developed by Puckett[22] to study hyperbolic flows. In this technique the error between the volume fractions given by the true and approximate interfaces is minimized by the least squares line fit to a 3×3 cell unit. Ashgriz and Poo[23] introduced the FLAIR technique, which is also based on a sloped line segment at the interface. FLAIR is different from other techniques in that the volume fraction is advected on the basis of the area beneath a portion of the interface line segment which lies near the boundary of two neighbouring cells. This technique has the advantage of generating a continuous interface at the cell boundaries. Ashgriz and Poo[23] showed that the FLAIR method is more accurate than the Hirt–Nichols[14] VOF method. There are other techniques which also use VOF in determining the interface advection, but they mainly vary based on their treatment of the interface boundary conditions. For example, Liang[24] combined a non-orthogonal body-fitted grid for the momentum calculation with VOF for interface advection.

VOF-based techniques have been used extensively to simulate axisymmetric free surface flows. Torrey *et al.*[25] have described a VOF-based algorithm which can simulate axisymmetric and three-dimensional flows. Golafshani[26] analysed axisymmetric transient creeping flows with free surfaces using the VOF method of Hirt and Nichols.[14]

Up to this point the essential differences between advection of volume fractions in Cartesian and axisymmetric co-ordinates have not been addressed properly. In this paper we have introduced a criterion for the advection of the volume fractions in axisymmetric co-ordinates. In Section 2 the criterion for interface advection is developed using first principles and the differences between 2D Cartesian and axisymmetric advections are defined. In Section 3 the shortcomings of the previous methods for handling axisymmetric interfaces are discussed. In Sections 4 and 5 the equations for advecting the volume fraction in the axial and radial directions are developed using the FLAIR technique. Finally, the performance of the present approach is illustrated in Section 6 by sample calculations.

2. ADVECTION CRITERION

Consider the cross-sectional view of the axisymmetric two-fluid system shown in Figure 1, in which the shaded area represents the volume occupied by fluid 1 and the region outside the shaded area represents the volume occupied by fluid 2. These two areas will be referred to as the fluid and no-fluid regions respectively. Therefore one can define a volume fraction parameter $f_{i,j}$ for each cell (i, j) which can take values between unity and zero, i.e. $f_{i,j} = 0$ represents an empty cell, $f_{i,j} = 1$ a full cell and $0 < f_{i,j} < 1$ an interface cell. A cell with $0 < f_{i,j} < 1$ will be called a 'wet cell'. The problem is to reconstruct the interface shape and to advect the interface by knowing the f-field and the velocity components in the z- and r-directions (u and v respectively).

By examining the fractional volumes in each cell pair in the axial direction, one of the conditions shown in Figure 2 can be identified. Each cell can be empty, wet or full and therefore the two neighbouring cells can have nine different combinations. For instance, if we define the volume fraction in the cell on the left as $f_{i,j}$ and that on the right as $f_{i+1,j}$, case Z-1 corresponds to $0 < f_{i,j} < 1$ and $f_{i+1,j} = 0$, case Z-2 corresponds to $f_{i,j} = 0$ and $0 < f_{i+1,j} < 1$ and case Z-9 corresponds to $0 < f_{i,j} < 1$ and $0 < f_{i+1,j} < 1$. The same can be said for the radial direction r when considering $f_{i,j}$ and $f_{i,j+1}$ as shown in Figure 3.

A criterion should be defined based on which the volume fractions can be advected spatially. Many of the previous advection techniques apply the continuity equation to each of the interior cells in the

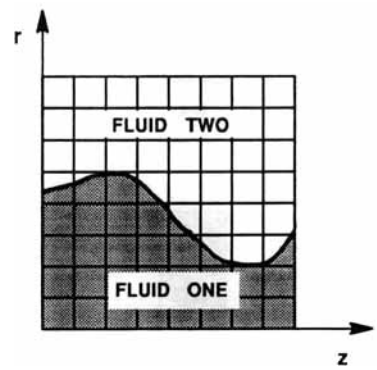

Figure 1. Two-fluid volume fraction field in Eulerian grid space

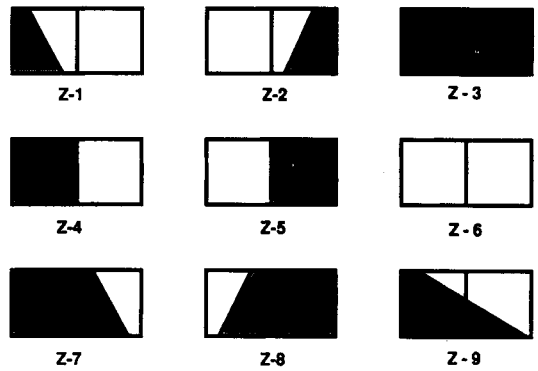

Figure 2. Possible cases of volume fractions for two neighbouring cells in the axial direction

system (i.e. full cells). However, for the interface cells, owing to the difficulty in direct application of the continuity equation, special techniques had to be developed. The generalized advection criterion described here consistently satisfies the continuity equation for all the cells including the interface cells. In order to develop this criterion, we have to resort to the standard procedure for the discretization of the continuity equation. Therefore consider the continuity equation for an incompressible fluid applied to the volume of a single cell,

$$\int_z \int_r \left(\frac{\partial u}{\partial z} + \frac{1}{r^\beta} \frac{\partial}{\partial r} (r^\beta v) \right) (2\pi r)^\beta \mathrm{d}r \, \mathrm{d}z = 0, \tag{1}$$

where $\beta = 0$ for Cartesian and $\beta = 1$ for axisymmetric co-ordinates.

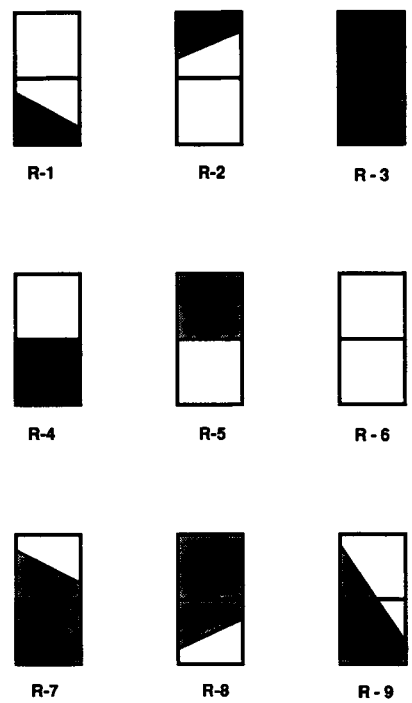

Figure 3. Possible cases of volume fractions for two neighbouring cells in the radial direction

In volume-tracking techniques the surface advection in each time step is carried out in each coordinate direction independently. For instance, in the axisymmetric case the volume fractions are first advected in the z-direction and then in the r-direction, and vice versa in the next time step. Therefore the integral in equation (1) resolves into two separate integrals (one in z and one in r). Since equation (1) includes partial derivatives for u and v, in order to be able to integrate this equation over one cell, some assumptions for the variation in u and v along the axes z and r are needed. The simplest assumptions that can be made are *u being independent of r and $r^\beta v$ being independent of z in each cell.* With these assumptions equation (1) can be written as

$$\int_r \int_z \left(\frac{\mathrm{d}u}{\mathrm{d}z}\mathrm{d}z\right)(2\pi r)^\beta \mathrm{d}r + \int_z \int_r \left(\frac{1}{r^\beta}\frac{\mathrm{d}(r^\beta v)}{\mathrm{d}r}(2\pi r)^\beta \mathrm{d}r\right)\mathrm{d}z = 0. \tag{2}$$

The velocities on the cell faces are defined in terms of the staggered grid shown in Figure 4. Assuming constant velocities during the time increment δt, equation (2) becomes

$$\begin{aligned}\int_{r_\mathrm{B}}^{r_\mathrm{T}} (u_{i+1/2,j}\delta t)(2\pi r)^\beta \mathrm{d}r - \int_{r_\mathrm{B}}^{r_\mathrm{T}} (u_{i-1/2,j}\delta t)(2\pi r)^\beta \mathrm{d}r \\ + \int_{z_\mathrm{L}}^{z_\mathrm{R}} (v_{i,j+1/2}\delta t)(2\pi r_{j+1/2})^\beta \mathrm{d}z - \int_{z_\mathrm{L}}^{z_\mathrm{R}} (v_{i,j-1/2}\delta t)(2\pi r_{j-1/2})^\beta \mathrm{d}z = 0,\end{aligned} \tag{3}$$

where the subscripts T, B, R and L refer to top, bottom, right and left limits of the integral for a cell respectively. These limits may vary depending on the location of the interface in the cell. For instance, for a full cell ($f_{i,j} = 1$) $r_\mathrm{B} = r_{j-1/2}$, $r_\mathrm{T} = r_{j+1/2}$, $z_\mathrm{L} = z_{i-1/2}$ and $z_\mathrm{R} = z_{i+1/2}$. In Sections 4 and 5 the cell volume fractions along with the location of the interface within the cell will be used to determine the limits of integration for the interface cells. Since each of the integrals in equation (3) represents the fluid flux across one of the cell faces, the initial assumptions for the derivation of equation (2) are in fact the advection criterion. Explicitly, we propose the following criterion for the advection of the volume fractions.

(i) *for axial advection, u = const. in the vicinity of each cell face*
(ii) *for radial advection, $r^\beta v$ = const. in the vicinity of each cell face.*

The advection criterion is directly extracted from equations (2) and (3) which include integrals of u and $r^\beta v$. Any other assumption for the variation in u and v with r and z in the vicinity of a cell face will

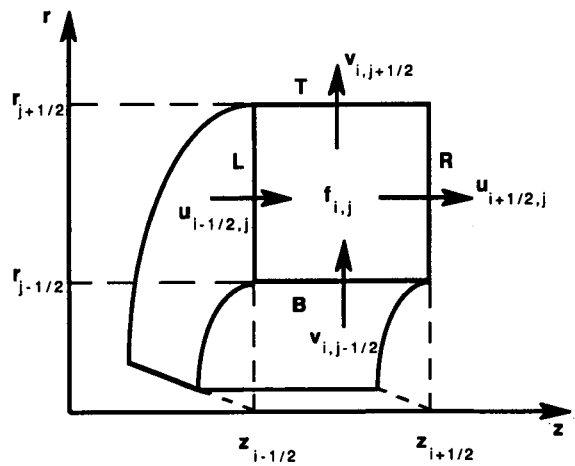

Figure 4. An axisymmetric cell with the cell velocities

make the algorithm much more complex. For instance, in order to evaluate the integrals in equation (3), one can assume $v/r = $ const. Applying this assumption to the continuity equation will result in $-u/2z = $ const. criterion. This assumption makes the algorithm more complex (since u is function of z).

3. COMPARISON WITH PREVIOUS ADVECTION CRITERION

The advection of the volume fraction field in almost all previous VOF-based methods has been based on the properties of a discontinuous interface. The interface is defined by a surface of discontinuity, $F(\mathbf{x},t)$, which is assumed to be a Lagrangian invariant and therefore satisfies the relation

$$\frac{DF}{Dt} = \frac{\partial F}{\partial t} + (\mathbf{U}\cdot\nabla)F = 0, \tag{4}$$

where $\mathbf{U}$ is the velocity vector. The surface function $F(\mathbf{x},t)$ is then related to the volume fraction field $f_{i,j}$. Equation (4) is subsequently divided into two parts[14]

$$\tilde{f} = f^n - \delta t\nabla\cdot(\mathbf{U}f^n) \tag{5}$$

$$f^{n+1} = \tilde{f} + \delta t(\nabla\cdot\mathbf{U})f^n, \tag{6}$$

in which f^{n+1} is the new advected cell volume fraction determined from its previous value f^n. Equation (6) basically provides a correction for the error in the momentum solver, since, for incompressible flow, $\nabla\cdot\mathbf{U} = 0$ and hence f^{n+1} becomes identical with $\tilde{f}$. Therefore equation (5) is used to define the advection of the volume fraction. This equation is later written in the form

$$\tilde{f}_{i,j} = f^n_{i,j} - \frac{\delta t}{\delta z}(u^{n+1}_{i+1/2,j}\langle f\rangle_R - u^{n+1}_{i-1/2,j}\langle f\rangle_L) - \frac{\delta t}{r_j\delta r}(r_{j+1/2}v^{n+1}_{i,j+1/2}\langle f\rangle_T - r_{j-1/2}v^{n+1}_{i,j-1/2}\langle f\rangle_B). \tag{7}$$

The bracketed quantities $\langle f\rangle$ are the fractional fluid volumes crossing each cell face; they were calculated based on the Hirt–Nichols[14] reconstruction algorithm. Equation (7) represents the mass conservation for each cell. The difficulty now resides in properly treating the volume fraction flux at the cell faces.

In order to obtain a physical interpretation of equation (7), consider the term which contributes to the advection in the r-direction at the top cell face. Multiplying the numerator and denominator of the first term in the second pair of brackets by $2\pi\delta z$ yields

$$\frac{2\pi r_{j+1/2}v^{n+1}_{i,j+1/2}\delta t\delta z\langle f\rangle_T}{2\pi r_j\delta r\delta z} = \frac{\text{volume advected}}{\text{total cell volume}}. \tag{8}$$

Comparing this with the third term in equation (3), the same expression $2\pi r_{j+1/2}v^{n+1}_{i,j+1/2}\delta t$ can be seen in both equations. For full cells, which are located inside the domain, $\langle f\rangle_T = 1$ in equation (8). Also, $z_L = z_{i-1/2}$ and $z_R = z_{i+1/2}$ in equation (7) and the integral from z_L to z_R equals the cell size δz. Therefore the two equations give the same volume change for full cells. For interface cells the quantity $2\pi r_{j+1/2}v_{i,j+1/2}\delta t$ can no longer be considered as the advected volume, because it may result in a volume change greater than the actual volume of fluid in the cell. In the previous VOF methods the term $\langle f\rangle$ was used to overcome this problem. The main difference between our approach to advect the interfaces and the previous techniques is in the description of $\langle f\rangle$. Previous methods assume $v = $ const. in the vicinity of an interface cell and, by considering the orientation of the interface line segment, derive a relation for $\langle f\rangle$. This is not consistent with their volume advection at interior cells in cylindrical co-ordinates, which assumes $rv = $ const. at the cell faces. The approach proposed here consistently uses the $rv = $ const. criterion for both the interface and the interior cells.

As an example of the difference between axisymmetric advection using $rv = \text{const.}$ and $v = \text{const.}$ consider the interface shown in Figure 5. The interface is defined by a line AB which intersects the left face of cell (i, j) at $r_A = 1{\cdot}6$ and the right face at $r_B = 2{\cdot}4$. For simplicity it is assumed that $u = 0$ and $v_{i,j+1/2}\delta t = 0{\cdot}4$. Therefore the volume of fluid in cell (i, j) is $V_{i,j} = 2{\cdot}6267\pi$, which results in $f_{i,j} = 0{\cdot}8756$ for cell sizes of unity. The volume of fluid in cell $(i, j+1)$ is $V_{i,j+1} = 0{\cdot}4267\pi$, resulting in $f_{i,j+1} = 0{\cdot}08533$. In previous VOF-based methods for axisymmetric co-ordinates, since $v_{i,j+1/2}\delta t = 0{\cdot}4$ is used as the distance that the interface is advected, the volume flux that can be obtained is the volume of section AONCA,

$$\Delta V_{\text{VOF}} = 2\pi r_j f_{i,j} - 2\pi r_{1{\cdot}3}(0{\cdot}6) = 1{\cdot}0667\pi, \tag{9}$$

which is the total volume of the fluid in cell (i, j) minus the volume of fluid in section ACRLA. However, the present technique using equation (3) results in

$$\Delta V_{\text{FLAIR}} = 2\pi r_{j+1/2} v_{i,j+1/2}\delta t - V_{\text{AOMA}} = 1{\cdot}2267\pi, \tag{10}$$

which is the exact volume flux advected during the time interval δt. Therefore VOF-based methods result in 13% error for the case shown in Figure 5. In order to correct for this error, special techniques had to be developed. For instance, the surface is further shifted to satisfy the conservation of mass for a domain of 3×3 cell units. By using $rv = \text{const.}$ as the advection criterion, no secondary correction model is needed.

4. INTERFACE RECONSTRUCTION IN AXIAL DIRECTION

The advection equations in axisymmetric systems are developed based on the FLAIR algorithm of Ashgriz and Poo.[23] While the method is applied only to the FLAIR technique, it is to be noted that the same procedure may be used to develop the flux equations for all other VOF-based interface advection models.

In contrast with 2D Cartesian co-ordinates, movements along the z- and r-directions in axisymmetric co-ordinates do not obey the same relations. Also in each co-ordinate system, different relations must be used depending on the positive or negative direction of the movement. In axisymmetric co-ordinates the relationships for the interface advection are more complicated and contain a greater number of

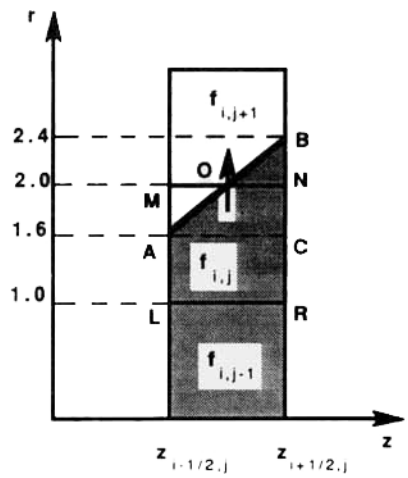

Figure 5. Volume fraction flux calculation for two neighbouring radial cells

independent variables. Consequently, unlike the 2D Cartesian case,[23] it is not possible to find closed form solutions in axisymmetric co-ordinates. Numerical solutions are required to determine the unknowns and distinction of the different cases must be accomplished on a trial-and-error basis.

The first step for interface advection is to identify the surface orientation from the f-field. In the FLAIR method this is accomplished by inspecting the volume fractions in two neighbouring cells as shown in Figure 2. Consider first advection in the z-direction. The most general case occurs when two neighbouring cells are both wet—shown in case Z-9 of Figure 2. All other cases for advection in the z-direction can be reduced to this case. Therefore case Z-9 is discussed first. Four possible conditions for case Z-9 are obvious by inspection. They are shown in Figure 6 as subcases Z-9-a–Z-9-d. The method for determining the interface line for subcase Z-9-a is discussed below and the results for the other subcases are treated in Appendix I. Assume that the cross-section of the interface in the r–z plane can be approximated by a line segment fitted through the boundary of two neighbouring cells such that

$$\eta = a_j \xi + b_j, \tag{11}$$

where the orthogonal co-ordinates (η, ξ) are attached to the lower left corner of cell (i, j) as shown in Figure 7. The constants a_j and b_j are to be determined from the known volume fractions $f_{i,j}$ and $f_{i+1,j}$ and the radius of the bottom cell face, $r_{j-1/2}$. The total volume of one cell is

$$V_j^c = \pi(r_{j+1/2}^2 - r_{j-1/2}^2)(z_{i+1/2} - z_{i-1/2}). \tag{12}$$

Hereinafter, cell sizes in the r- and z-directions are assumed to be equal to unity ($\delta r = \delta z = 1$). Variable grid sizes can be considered in the same manner, but the equations cannot be simplified. For a grid which is uniform in both r- and z-directions, equation (12) reduces to

$$V_j^c = \pi(2r_{j-1/2} + 1). \tag{13}$$

It should be emphasized that V_j^c varies with $r_{j-1/2}$. The wetted volumes in the two cells are

$$V_{i,j} = \tfrac{1}{3}\pi(1)[(r_{j-1/2} + b_j)^2 + (r_{j-1/2} + b_j)(r_{j-1/2} + a_j + b_j) + (r_{j-1/2} + a_j + b_j)^2 - 3r_{j-1/2}^2],$$

$$V_{i+1,j} = \tfrac{1}{3}\pi(1)[(r_{j-1/2} + a_j + b_j)^2 + (r_{j-1/2} + a_j + b_j)(r_{j-1/2} + 2a_j + b_j) + (r_{j-1/2} + 2a_j + b_j)^2 - 3r_{j-1/2}^2].$$

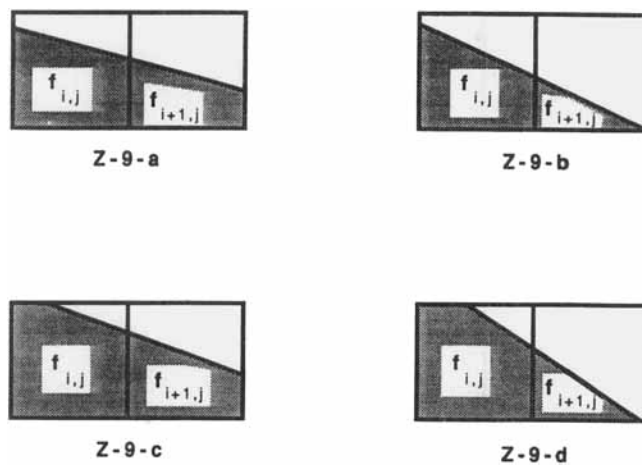

Figure 6. Four possible cases of interface orientation for case Z-9

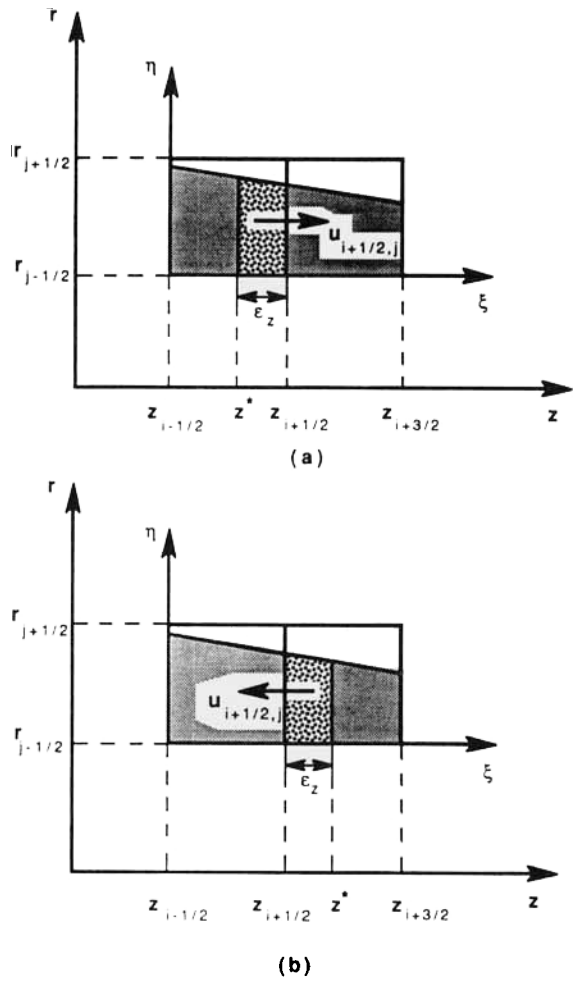

Figure 7. Volume fraction flux calculation for two neighbouring cells in (a) positive and (b) negative axial directions

The volume fractions then become

$$f_{i,j} = \frac{V_{i,j}}{V_j^c} = \frac{1}{3(2r_{j-1/2}+1)}[(r_{j-1/2}+b_j)^2 + (r_{j-1/2}+b_j)(r_{j-1/2}+a_j+b_j) + (r_{j-1/2}+a_j+b_j)^2 - 3r_{j-1/2}^2], \tag{14}$$

$$f_{i+1,j} = \frac{V_{i+1,j}}{V_j^c} = \frac{1}{3(2r_{j-1/2}+1)}[(r_{j-1/2}+a_j+b_j)^2 + (r_{j-1/2}+a_j+b_j)(r_{j-1/2}+2a_j+b_j) + (r_{j-1/2}+2a_j+b_j)^2 - 3r_{j-1/2}^2]. \tag{15}$$

Equations (14) and (15) may be written in the forms

$$\varphi(a_j,\ b_j) = (r_{j-1/2}+b_j)^2 + (r_{j-1/2}+b_j)(r_{j-1/2}+a_j+b_j) + (r_{j-1/2}+a_j+b_j)^2 - [3r_{j-1/2}^2 + 3f_{i,j}(2r_{j-1/2}+1)] = 0, \tag{16}$$

$$\psi(a_j, b_j) = (r_{j-1/2} + a_j + b_j)^2 + (r_{j-1/2} + a_j + b_j)(r_{j-1/2} + 2a_j + b_j) + (r_{j-1/2} + 2a_j + b_j)^2 - [3r_{j-1/2}^2 + 3f_{i+1,j}(2r_{j-1/2} + 1)] = 0, \quad (17)$$

which constitute a set of coupled non-linear equations in the two unknowns a_j and b_j. In each time step these equations are solved numerically using the Newton–Raphson method.

Once the surface has been reconstructed, the fluid flux moving from one cell to the neighbouring cell can be calculated by integrating the volume in the shell which is contained between the bottom of the cells and the interface line. The length of this shell is $\varepsilon_z = |u_{i+1/2,j}\delta t|$, which is the distance that the fluid is advected in the z-direction during the time interval δt. By using equation (3) for the z-direction, it follows that

$$\Delta V_{i,j} = \int_{z^*}^{z_{i+1/2}} \int_{r_{j-1/2}}^{r_{j-1/2}+\eta(\xi)} 2\pi r \, dr \, dz, \quad (18)$$

where z^* is defined as $z^* = z_{i+1/2} - \varepsilon_z$. Figures 7(a) and 7(b) show the effective areas for positive and negative z-fluxes respectively. Knowing a_j, b_j, and $r_{j-1/2}$, the fluid fluxes for positive and negative movements may be shown to be

$$\delta f_{i,j}^{+} = \frac{\varepsilon_z}{3(2r_{j-1/2}+1)}[(r_{j-1/2} + a_j - a_j\varepsilon_z + b_j)^2 + (r_{j-1/2} + a_j - a_j\varepsilon_z + b_j) \times (r_{j-1/2} + a_j + b_j) + (r_{j-1/2} + a_j + b_j)^2 - 3r_{j-1/2}^2], \quad (19)$$

$$\delta f_{i,j}^{-} = \frac{\varepsilon_z}{3(2r_{j-1/2}+1)}[(r_{j-1/2} + a_j + a_j\varepsilon_z + b_j)^2 + (r_{j-1/2} + a_j + a_j\varepsilon_z + b_j) \times (r_{j-1/2} + a_j + b_j) + (r_{j-1/2} + a_j + b_j)^2 - 3r_{j-1/2}^2]. \quad (20)$$

Since closed form solutions do not exist for a_j and b_j, the case at hand cannot be recognized in advance from the values of $f_{i,j}$, $f_{i+1,j}$, and $r_{j-1/2}$. For every set of $f_{i,j}$, $f_{i+1,j}$, and $r_{j-1/2}$, the computations are started with subcase Z-9-a. After a_j and b_j have been found, the size limits shown in Figure 6 are checked for that subcase. For instance, the size limits for subcase Z-9-a are $0 \leqslant \eta(0) \leqslant 1$ and $0 \leqslant \eta(2) \leqslant 1$. If the size limits are satisfied, then subcase Z-9-a is the correct one, otherwise different cases must be tried in the same way. It is possible that the 'heavy' side of the two neighbouring cells (the side where more fluid is located) is other than the one shown in subcase Z-9-a. In such cases the volume fractions $f_{i,j}$ and $f_{i+1,j}$ are redefined such that one of the surfaces shown in Figure 6 is recovered.

In cases Z-3–Z-6 of Figure 2 the cells are either full or empty and therefore the surface orientation is known. For other cases, e.g. Z-1, the line segment must be found within the cell rather than at the cell boundary. Figure 8 shows all possible cases for a single wet cell. Cases I-a–I-d are independent and are investigated in detail in Appendix I and the other cases can be reduced to them by co-ordinate transformation. The slope of the line segment in these cases is determined by taking the average of the slopes found at the cell boundaries between the wet cell under consideration and its neighbouring wet cells. Then, knowing the volume fraction $f_{i,j}$, the average slope $\bar{\theta}$ and the radius of the bottom cell face, $r_{j-1/2}$, the criterion developed in Appendix I is used to identify the type of wet cell. The derivation of the volume fraction fluxes for these cases is also presented in Appendix I.

5. INTERFACE RECONSTRUCTION IN RADIAL DIRECTION

The procedure for distinguishing the cases in the radial direction is similar to that in the axial direction. All possible cases for two neighbouring cells are shown in Figure 3. Similarly to the axial advection

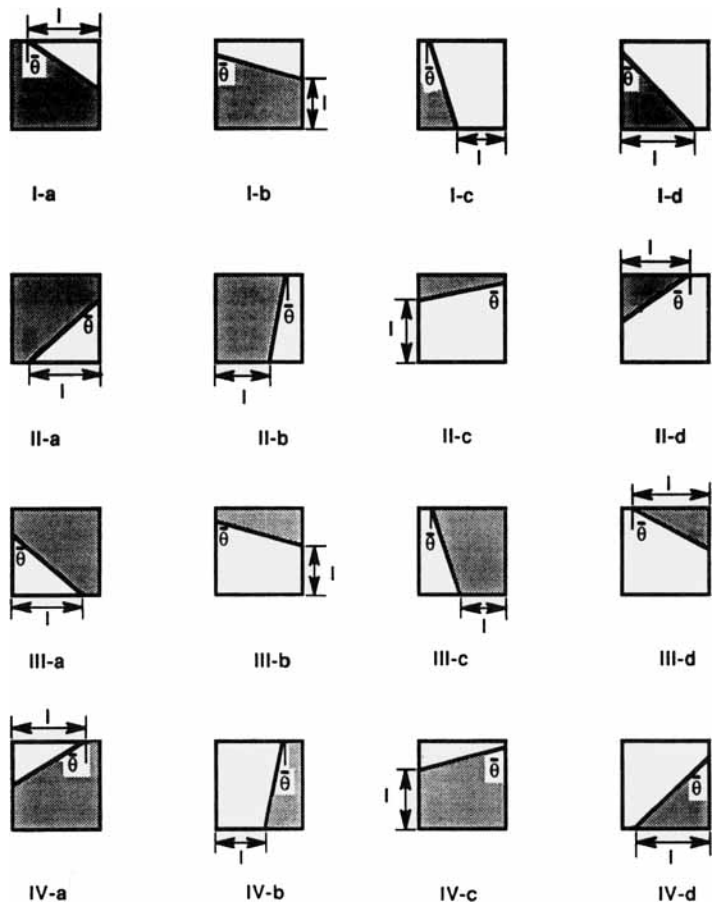

Figure 8. Sixteen possible cases for the interface orientation and heavy side of a single interface cell

case, the most general case is R-9, which has four subcases as shown in Figure 9. If the heavy sides are other than the left faces of the cells, the volume fractions are redefined such that the subcases shown in Figure 9 are obtained. The interface orientation in cases R-3–R-6 is known in advance, since the cells are either full or empty. In the remaining cases the interface should be found in a single wet cell. In a circumstance such as case R-1 the slope of the interface is evaluated as an average of the interface slopes in the neighbouring cells. Knowing the volume fraction $f_{i,j}$ and the slope $\bar{\theta}$, one of the cases

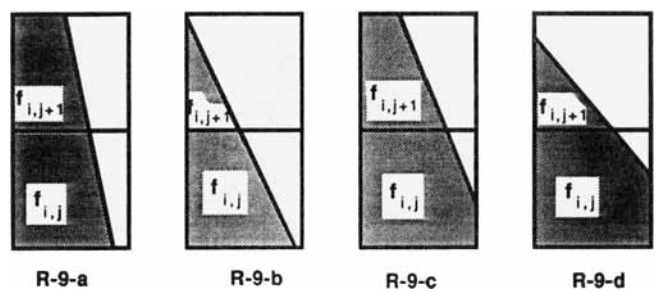

Figure 9. Four possible cases for the interface orientation of two neighbouring cells in the radial direction for case R-9

shown in Figure 8 can be identified for the wet cell, as described previously for z-direction interface reconstruction.

For advection in the axial direction the wetted volumes of each cell, $V_{i,j}$, are reduced to the fractional volumes $f_{i,j}$ by dividing them by the total volume of the cell, V_j^c (see equations (14) and (15)). Since the cell volume V_j^c stays constant during axial advection at any $r_{j-1/2}$, the volume fraction flux $\delta f_{i,j}$ could be used for the interface advection. However, for advection in the radial direction the total volumes of the neighbouring cells are different. Since the f-field is advected by taking a total *volume flux* ΔV from one cell to the neighbouring one, the *volume fraction flux* δf will be different in each neighbouring radial cell. In order to circumvent this problem, the wetted volumes and the volume flux, rather than the volume fraction flux, are used in the advection of the f-field in the radial direction. Consider the downward advection of the fluid shown in Figure 10. From the continuity equation (3) the volume flux crossing the bottom cell face in the radial direction is given by

$$\int_{z_{i-1/2}}^{z_{i+1/2}} (v_{i,j-1/2}\delta t)2\pi r_{j-1/2}\,\mathrm{d}z = \int_0^1 2\pi\varepsilon_r r_{j-1/2}\mathrm{d}\xi, \tag{21}$$

where $\varepsilon_r = |v_{i,j-1/2}\delta t|$. Defining $\eta = \mathscr{G}(\xi)$ to be the vertical distance between the interface and the ξ-axis, the differential volume of fluid enclosed in the interval $\mathrm{d}\xi$ is

$$\mathrm{d}V_\eta = \pi(\eta^2 + 2r_{j-1/2}\eta)\,\mathrm{d}\xi \tag{22}$$

and the differential volume defined by equation (21) is

$$\mathrm{d}V_{\varepsilon_r} = 2\pi\varepsilon_r r_{j-1/2}\,\mathrm{d}\xi. \tag{23}$$

In evaluating the integral of equation (21), the volumes defined by equations (22) and (23) must be compared. The value of η_e for which the two volumes are equal is

$$\eta_e = \sqrt{(r_{j-1/2}^2 + 2r_{j-1/2}\varepsilon_r)} - r_{j-1/2} \tag{24}$$

and therefore $\xi_e = \mathscr{G}^{-1}(\eta_e)$ in the limit $\mathrm{d}V_\eta = \mathrm{d}V_{\varepsilon_r}$. The behaviour of the integral in equation (21) is different on either side of this limit. Let the volume of fluid enclosed in the interval from $\xi = 0$ to ξ be defined as $V(\xi)$. Then

$$\int_0^1 \mathrm{d}V = \begin{cases} \displaystyle\int_0^{\xi_e} \mathrm{d}V_{\varepsilon_r} = 2\pi r_{j-1/2}\varepsilon_r\xi_e & \text{if } 0 \leqslant \xi \leqslant \xi_e, \\ \displaystyle\int_{\xi_e}^1 \mathrm{d}V_\eta = V(\xi = 1) - V(\xi = \xi_e) & \text{if } \xi_e > \xi \geqslant 1 \end{cases}$$

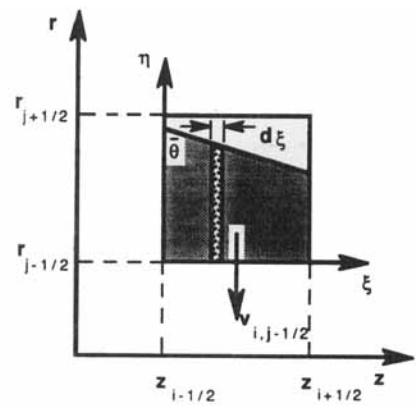

Figure 10. Volume flux calculation in the radial direction

and the total volume flux becomes

$$\Delta V = 2\pi r_{j-1/2}\varepsilon_r \xi_e + V(\xi = 1) - V(\xi = \xi_e). \tag{25}$$

Equation (25) is the general result for the advection of the volumes in the radial direction. For each case and its subcases the values of $\mathscr{G}(\xi)$, ξ_e and $V(\xi)$ are first determined and then the volume flux is calculated from equation (25). For instance, for downward advection in case I-a (see Figure 10) $\mathscr{G}(\xi)$, ξ_e and $V(\xi)$ become

$$\eta = \mathscr{G}(\xi) = \left(1 - \frac{l}{\theta}\right) + \frac{1-\xi}{\theta} \quad \text{for } \xi \geqslant 1 - l,$$

$$\xi_e = 1 - \theta(\eta_e + l\theta - 1),$$

$$V(\xi) = \begin{cases} \pi(2r_{j-1/2} + 1)\xi & \text{if } \xi \leqslant 1 - l, \\ (2r_{j-1/2} + 1)(1-l)\pi + \dfrac{\pi(\xi + l - 1)}{3}\left[(r_{j-1/2} + 1)^2 + (r_{j-1/2} + 1)\right. & \\ \left. \times \left(r_{j-1/2} + 1 - \dfrac{\xi + l - 1}{\theta}\right) + \left(r_{j-1/2} + 1 - \dfrac{\xi + l - 1}{\theta}\right)^2 - 3r_{j-1/2}^2\right], & \end{cases} \tag{26}$$

where $\theta = \tan\bar{\theta}$ and l and $\bar{\theta}$ are defined in Figure 8. This figure also shows that there are 16 different cases for a single wet cell. Cases I-a–I-d are the basic cases for downward advection and cases III-a–III-d may be reduced to these cases through simple transformation. Similarly, cases II-a–II-d are the basic cases for upward advection and cases IV-a–IV-d reduce to these by transformation. The same results are also utilized in flux calculations for cell pairs in the r-direction. The advection equations for the basic cases in the radial direction are given in Appendix II.

6. SAMPLE CALCULATIONS

The technique described in the previous sections, which is referred to as A-FLAIR (axisymmetric flux line segment model for advection and interface reconstruction), is implemented in several test problems for which advections of a circle located at various points in an axisymmetric Eulerian co-ordinate system are required. The initial circles, located at different positions, are moved with positive and/or negative velocities which satisfy the axisymmetric continuity equation. The radius of the initial circle is 25 in all cases.

Figure 11 shows the displacement of a circle in the radial direction when the axial velocities are set equal to zero. With this assignment for u, continuity requires that $rv = c$, where c is a constant. The exact motion of each point of a circle initially located at radius r_0 from the z-axis with the constraint $rv = c$ can be obtained by

$$r_f = \sqrt{(r_0^2 + 2ct)},$$

where r_f is the radial position of the point at time t. In Figure 11 the exact results given by the above equation for $c = 0{\cdot}8$ and $t = 1060$ are compared with the results obtained by A-FLAIR. Excellent agreement is attained. Also shown in Figure 11 is the final shape of the circle produced by direct application of the FLAIR technique[23] to the axisymmetric geometry. In this case the velocities for the interface advection were obtained using $rv = 0{\cdot}8$. The deviation from the analytical result is clearly seen, indicating that this approach does not satisfy the continuity equation applied to the interface cells.

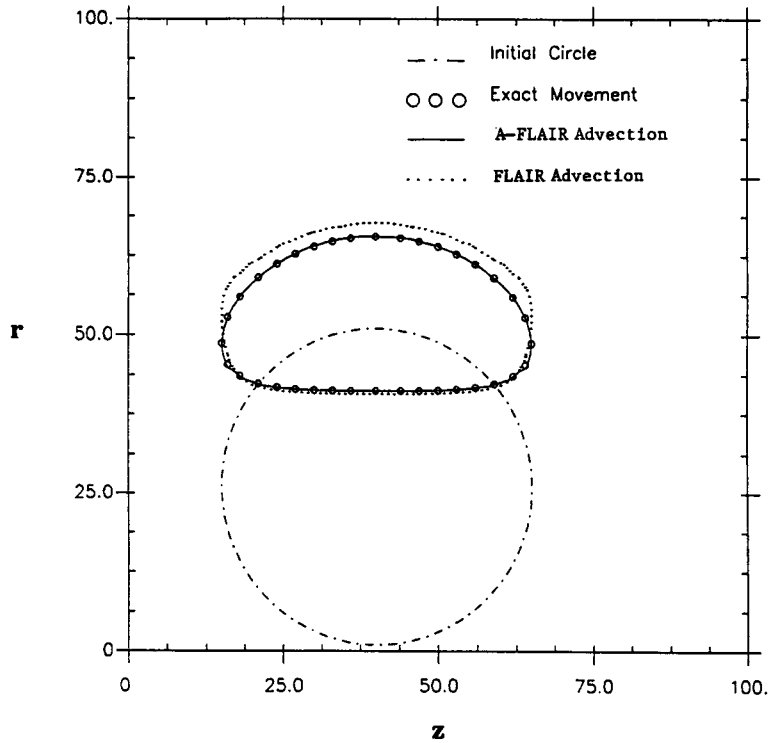

Figure 11. Advection of a circle in the positive radial direction

In order to reach the same final time used for evaluating the analytical result ($t = 1060$), a larger number of time steps (104 steps) had to be used for FLAIR advection than for A-FLAIR advection (100 steps). Since the error is larger at smaller radii, as shown in Section 3, the advection of the lower part of the circle is always predicted with less accuracy. Hence care must be exercised in interpreting the nature of the errors when looking at a figure such as Figure 11.

The initial circle shown in Figure 12(a) was allowed to perform a combined axial and radial displacement while having $u = 0{\cdot}4$ and $rv = 0{\cdot}8$. The final shape after 100 time steps of $\delta t = 1$ contained no deformation due to movement in the z-direction. However, in the r-direction the points at smaller r, having larger v, moved faster than the points at larger r. In Figure 12(b) a circle was moved in the negative z- and r-directions while having $u = -0{\cdot}4, rv = -10{\cdot}0$ and $\delta t = 1$ for each time increment. The points at smaller radii attained velocities which were relatively large compared with the velocities of the points located at larger radii.

A more stringent case was also considered by moving the test circle in a highly strained field of a single pinned vortex ring. The equations for the axial and radial velocities for the vortex ring are given by[27]

$$u = \frac{\Gamma\bar{R}}{4\pi r}\frac{2(l-r)}{a^2}\left(1+\frac{5(r-l)}{4\bar{R}}\right)+\frac{\Gamma}{4\pi r}\left[\log\left(\frac{8\bar{R}}{a}\right)+1-\frac{5}{4a^2}(z^2+r^2-2lr+l^2)\right], \tag{27}$$

$$v = \frac{\Gamma\bar{R}z}{2\pi a^2 r}\left(1+\frac{5(r-l)}{4\bar{R}}\right), \tag{28}$$

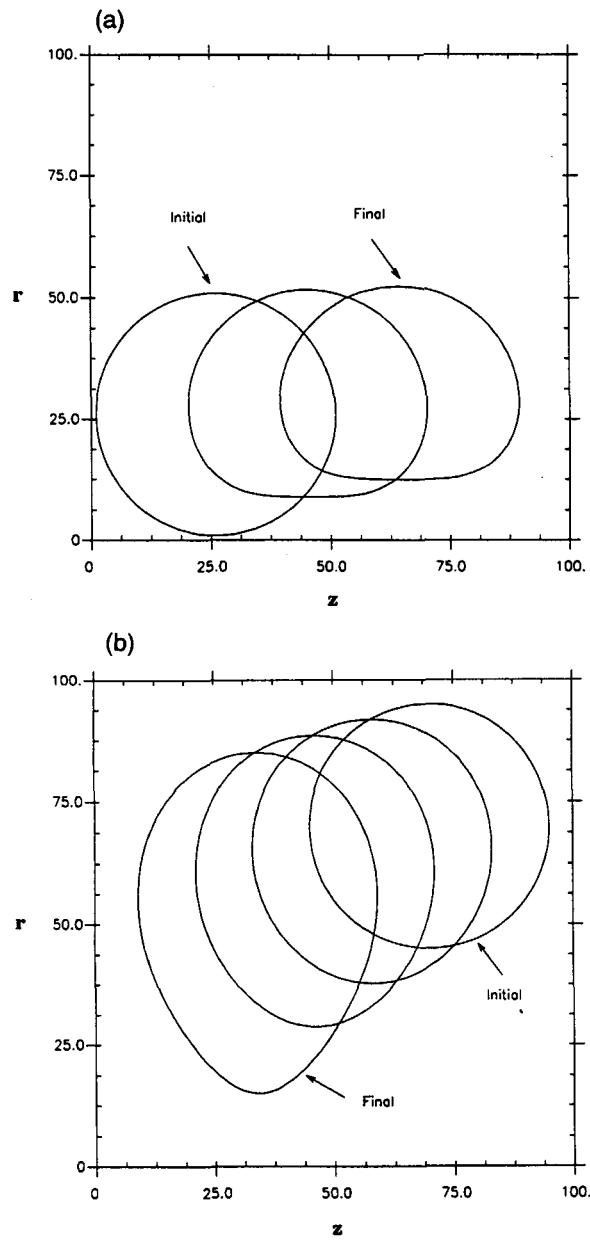

Figure 12. Advection of a circle in combined radial and axial directions: (a) positive and (b) negative velocities

where $\Gamma, \bar{R}, a$ and l are the total circulation about the core, the radius of the centroid, the core radius and the radial distance of the co-ordinate attached to the ring from the axis of symmetry[27] respectively. For the sample case we chose $\Gamma = -0{\cdot}4, \bar{R} = 140, a = 4$ and $l = 140$. Figure 13 shows the velocity field for the region under consideration along with the initial circle and four successive snapshots of evolved shapes. The accuracy of the advection technique is tested against the exact displacement of different points by numerically integrating equations (27) and (28). The results of the exact solution are

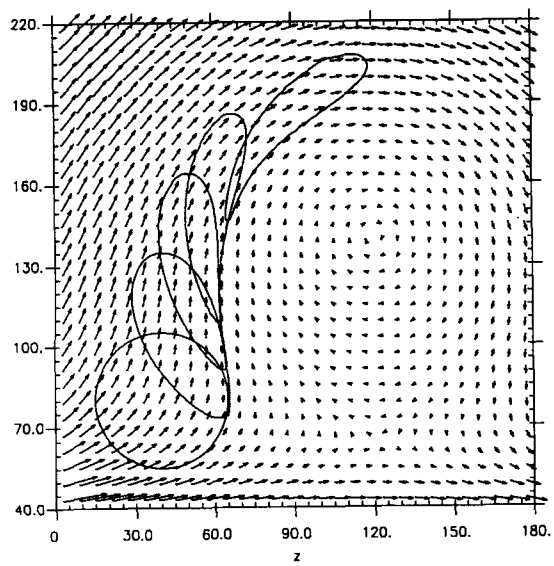

Figure 13. Advection of a circle in a flow field generated by a pinned single vortex ring. The corresponding times are 0, 98·12, 193·87, 279·71 and 443·58

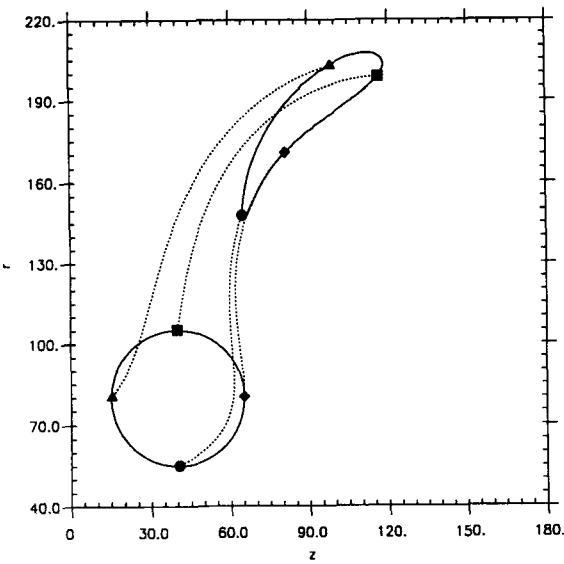

Figure 14. Comparison of the A-FLAIR results with the exact solution. Dotted lines represent the particle path

compared with the results of A-FLAIR in Figure 14, which shows excellent agreement. The volume change was also calculated for these cases and the average change in volume during each time step was found to be 10^{-7}, which can be redistributed in the two cells.

ACKNOWLEDGEMENTS

This work was supported by the Fluid Particulates and Hydraulic Systems Division of the NSF under grant number CTS-9011201. Also, comments and suggestions of Professor J. D. Felske are gratefully acknowledged.

APPENDIX I: VOLUME FLUX ADVECTION IN THE AXIAL DIRECTION

Subcase Z-9-b

Let l_b be the distance from the intersection point of the interface line with the cell bottom to the common face of the two cells as shown in Figure 15(a). Then

$$l_b = -\left(1 + \frac{b_j}{a_j}\right).$$

Using the same procedure as in subcase Z-9-a, it follows that

$$\varphi(a_j, b_j) = (r_{j-1/2} + b_j)^2 + (r_{j-1/2} + b_j)(r_{j-1/2} + a_j + b_j) + (r_{j-1/2} + a_j + b_j)^2 - [3r_{j-1/2}^2 + 3f_{i,j}(2r_{j-1/2} + 1)] = 0,$$

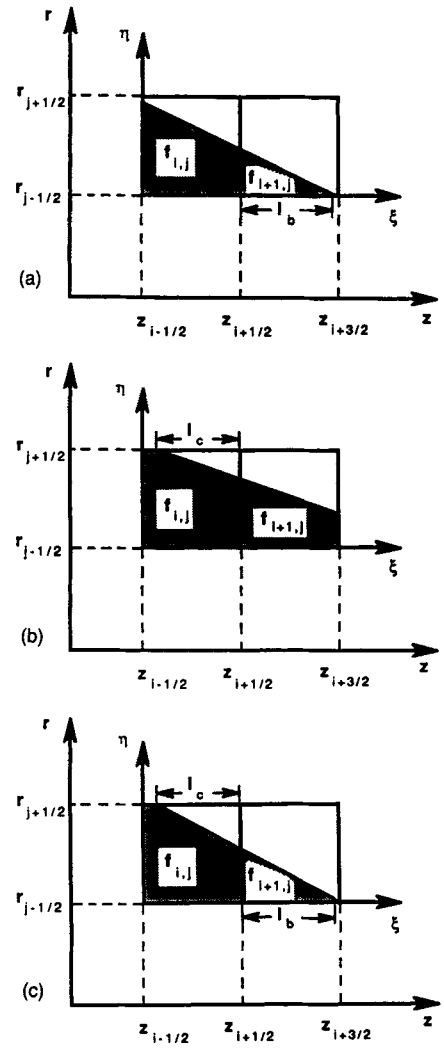

Figure 15. Interface orientation for (a) subcase Z-9-b, (b) subcase Z-9-c and (c) subcase Z-9-d

$$\psi(a_j, b_j) = (a_j + b_j)[(r_{j-1/2} + a_j + b_j)^2 + (a_j + b_j)r_{j-1/2} - r_{j-1/2}^2] + 3f_{i+1,j}a_j(2r_{j-1/2} + 1) = 0$$

and the volume fraction fluxes are given by

$$\delta f^+ = \frac{\varepsilon_z}{3(2r_{j-1/2} + 1)}[(r_{j-1/2} + a_j - a_j\varepsilon_z + b_j)^2 + (r_{j-1/2} + a_j - a_j\varepsilon_z + b_j) \times (r_{j-1/2} + a_j + b_j) + (r_{j-1/2} + a_j + b_j)^2 - 3r_{j-1/2}^2],$$

$$\delta f^- = \begin{cases} f_{i+1,j} & \text{if } \varepsilon_z \geqslant l_b, \\ \dfrac{\varepsilon_z}{3(2r_{j-1/2}+1)}[(r_{j-1/2}+a_j+a_j\varepsilon_z+b_j)^2+(r_{j-1/2}+a_j+a_j\varepsilon_z+b_j) \\ \qquad \times(r_{j-1/2}+a_j+b_j)+(r_{j-1/2}+a_j+b_j)^2-3r_{j-1/2}^2], & \text{if } \varepsilon_z \leqslant l_b. \end{cases}$$

Subcase Z-9-c

Similarly, defining l_c as shown in Figure 15(b), it follows that

$$l_c = 1 + \frac{b_j - 1}{a_j},$$

$$\varphi(a_j, b_j) = 3(2r_{j-1/2}+1)(1-b_j)+(a_j+b_j-1)[(r_{j-1/2}+1)^2+(r_{j-1/2}+1)(r_{j-1/2}+a_j+b_j) + (r_{j-1/2}+a_j+b_j)^2-3r_{j-1/2}^2]-3a_jf_{i,j}(2r_{j-1/2}+1)=0,$$

$$\psi(a_j, b_j) = (r_{j-1/2}+a_j+b_j)^2+(r_{j-1/2}+a_j+b_j)(r_{j-1/2}+2a_j+b_j) + (r_{j-1/2}+2a_j+b_j)^2-[3r_{j-1/2}^2+3f_{i+1,j}(2r_{j-1/2}+1)]=0$$

and the volume fraction fluxes are given by

$$\delta f^+ = \begin{cases} \varepsilon_z + f_{i,j} - 1 & \text{if } \varepsilon_z \geqslant l_c, \\ \dfrac{\varepsilon_z}{3(2r_{j-1/2}+1)}[(r_{j-1/2}+a_j-a_j\varepsilon_z+b_j)^2+(r_{j-1/2}+a_j-a_j\varepsilon_z+b_j) \\ \qquad \times(r_{j-1/2}+a_j+b_j)+(r_{j-1/2}+a_j+b_j)^2-3r_{j-1/2}^2] & \text{if } \varepsilon_z < l_c, \end{cases}$$

$$\delta f^+ = \frac{\varepsilon_z}{3(2r_{j-1/2}+1)}[(r_{j-1/2}+a_j+a_j\varepsilon_z+b_j)^2+(r_{j-1/2}+a_j+a_j\varepsilon_z+b_j)(r_{j-1/2}+a_j+b_j) + (r_{j-1/2}+a_j+b_j)^2-3r_{j-1/2}^2].$$

Subcase Z-9-d

For this subcase l_b and l_c are defined in Figure 15(c) as

$$l_b = -\left(1+\frac{b_j}{a_j}\right), \qquad l_c = 1+\frac{b_j-1}{a_j}.$$

Then

$$\varphi(a_j, b_j) = 3(2r_{j-1/2}+1)(1-b_j)+(a_j+b_j-1)[(r_{j-1/2}+1)^2+(r_{j-1/2}+1)(r_{j-1/2}+a_j+b_j) + (r_{j-1/2}+a_j+b_j)^2-3r_{j-1/2}^2]-3a_jf_{i,j}(2r_{j-1/2}+1)=0,$$

$$\psi(a_j, b_j) = (a_j+b_j)[(r_{j-1/2}+a_j+b_j)^2+(a_j+b_j)r_{j-1/2}-r_{j-1/2}^2]+3f_{i+1,j}a_j(2r_{j-1/2}+1)=0$$

and the volume fraction fluxes are given by

$$\delta f^+ = \begin{cases} \varepsilon_z + f_{i,j} - 1 \quad \text{if } \varepsilon_z \geqslant l_c, \\ \dfrac{\varepsilon_z}{3(2r_{j-1/2}+1)}[(r_{j-1/2}+a_j-a_j\varepsilon_z+b_j)^2+(r_{j-1/2}+a_j-a_j\varepsilon_z+b_j) \\ \qquad \times(r_{j-1/2}+a_j+b_j)+(r_{j-1/2}+a_j+b_j)^2-3r_{j-1/2}^2] \quad \text{if } \varepsilon_z < l_c, \end{cases}$$

$$\delta f^- = \begin{cases} f_{i+1,j} \quad \text{if } \varepsilon_z \geqslant l_b, \\ \dfrac{\varepsilon_z}{3(2r_{j-1/2}+1)}[(r_{j-1/2}+a_j+a_j\varepsilon_z+b_j)^2+(r_{j-1/2}+a_j+a_j\varepsilon_z+b_j) \\ \qquad \times(r_{j-1/2}+a_j+b_j)+(r_{j-1/2}+a_j+b_j)^2-3r_{j-1/2}^2] \quad \text{if } \varepsilon_z < l_b. \end{cases}$$

Subcase I-a

When considering single wet cells, 16 different cases are possible as shown in Figure 8. The advection for all these cases in the axial direction can be reduced to the first four cases, namely cases I-a–I-d. For subcase I-a, evaluating the volume fraction $f_{i,j}$ based on $r_{j-1/2}$, $\bar{\theta}$ and l (as shown in Figure 8) and rearranging results in

$$l^3 - 3\theta(r_{j-1/2}+1)l^2 + 3\theta^2(2r_{j-1/2}+1)(1-f_{i,j}) = 0,$$

where $\theta = \tan\bar{\theta}$; l can be found from the above equation. The fluid flux may then be calculated in the same manner as for the cell pair cases. This leads to

$$\delta f = \begin{cases} \varepsilon_z + f_{i,j} - 1 \quad \text{if } \varepsilon_z \geqslant l, \\ \dfrac{\varepsilon_z}{3(2r_{j-1/2}+1)}\left[\left(r_{j-1/2}+1+\dfrac{\varepsilon_z-l}{\theta}\right)^2+\left(r_{j-1/2}+1+\dfrac{\varepsilon_z-l}{\theta}\right)\left(r_{j-1/2}+1-\dfrac{l}{\theta}\right)\right. \\ \qquad \left.+\left(r_{j-1/2}+1-\dfrac{l}{\theta}\right)^2-3r_{j-1/2}^2\right] \quad \text{if } \varepsilon_z < l. \end{cases}$$

Subcase I-b

This subcase refers to a single wet cell with $\pi/4 \leqslant \bar{\theta} \leqslant \pi/2$ as shown in Figure 8. The equation for l is

$$(r_{j-1/2}+l)^2 + \frac{1}{\theta}(r_{j-1/2}+l) + \frac{1}{3\theta^2} - r_{j-1/2}^2 - f_{i,j}(2r_{j-1/2}+1) = 0$$

and the volume fraction flux is given by

$$\delta f = \frac{\varepsilon_z}{3(2r_{j-1/2}+1)}\left[\left(r_{j-1/2}+l+\frac{\varepsilon_z}{\theta}\right)^2+\left(r_{j-1/2}+l+\frac{\varepsilon_z}{\theta}\right)(r_{j-1/2}+l)+(r_{j-1/2}+l)^2-3r_{j-1/2}^2\right].$$

Subcase I-c

As shown in Figure 8, l for this subcase is defined as the distance from the intersection point of the interface with the bottom cell face to the right cell face. It is given by

$$l = 1 - f_{i,j} - \frac{3r_{j-1/2} + 2}{3(2r_{j-1/2} + 1)}\theta$$

and the volume fraction flux for this case becomes

$$\delta f = \begin{cases} 0 \quad \text{if } \varepsilon_z \leqslant l, \\ \varepsilon_z + f_{i,j} - 1 \quad \text{if } \varepsilon_z \geqslant l + \theta, \\ \dfrac{\varepsilon_z - l}{3(2r_{j-1/2} + 1)} \left[\left(r_{j-1/2} + \dfrac{\varepsilon_z - l}{\theta} \right)^2 + \left(r_{j-1/2} + \dfrac{\varepsilon_z - l}{\theta} \right) r_{j-1/2} - 2r_{j-1/2}^2 \right] \\ \qquad \text{if } l < \varepsilon_z < l + \theta. \end{cases}$$

Subcase I-d

In this subcase a cubic equation results for l, i.e.

$$l^3 + 3r_{j-1/2}\theta l^2 - 3f_{i,j}\theta^2(2r_{j-1/2} + 1) = 0,$$

and the volume fraction flux becomes

$$\delta f = \begin{cases} 0 \quad \text{if } \varepsilon_z \leqslant 1 - l, \\ \dfrac{\varepsilon_z + l - 1}{3(2r_{j-1/2} + 1)} \left[\left(r_{j-1/2} + \dfrac{\varepsilon_z + l - 1}{\theta} \right)^2 + \left(r_{j-1/2} + \dfrac{\varepsilon_z + l - 1}{\theta} \right) r_{j-1/2} - 2r_{j-1/2}^2 \right] \\ \qquad \text{if } \varepsilon_z > 1 - l. \end{cases}$$

Once l has been found, the case is identified through a trial-and-error scheme by applying the size limits shown in Figure 8.

APPENDIX II: VOLUME FLUX ADVECTION IN THE RADIAL DIRECTION

II.1. Interface reconstruction in the radial direction

In this appendix the equations for the interface orientation are provided followed by the equations for the volume flux from one cell to its neighbour. Note that the general forms of the interface orientation for two neighbouring radial cells are shown in Figure 3. However, they can either be readily identified or be reduced to the case R-9. This case has four possible subcases which are shown in Figure 9 and will be discussed here.

Subcase R-9-a

Denote the cross-section of the interface in a cell pair on the r–z plane by the line

$$\xi = a_i\eta + b_i.$$

For subcase R-9-a shown in Figure 16(a) the volume fractions $f_{i,j}$ and $f_{i,j+1}$ are calculated from a_i, b_i and $r_{j-1/2}$ as

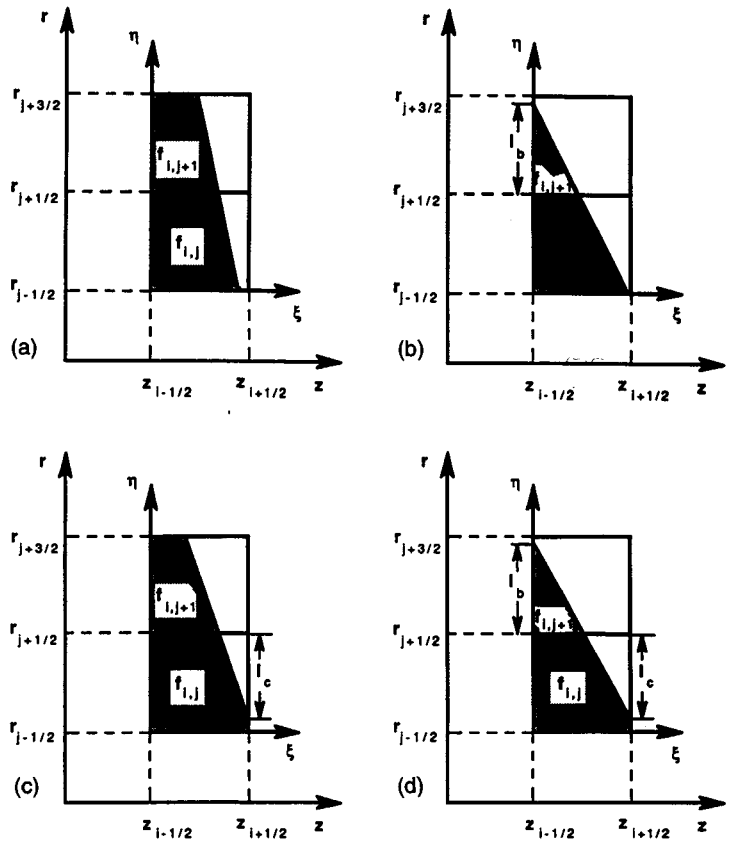

Figure 16. Interface orientation for (a) subcase R-9-a, (b) subcase R-9-b, (c) subcase R-9-c and (d) subcase R-9-d

$$f_{i,j} = \frac{3r_{j-1/2} + 2}{3(2r_{j-1/2} + 1)} a_i + b_i,$$

$$f_{i,j+1} = \frac{3r_{j-1/2} + 5}{3(2r_{j-1/2} + 3)} a_i + a_i + b_i$$

Solving these equations for a_i and b_i gives

$$a_i = \frac{f_{i,j+1} - f_{i,j}}{(9r_{j-1/2} + 14)/3(2r_{j-1/2} + 3) - (3r_{j-1/2} + 2)/3(2r_{j-1/2} + 1)},$$

$$b_i = f_{i,j} - \frac{3r_{j-1/2} + 2}{3(2r_{j-1/2} + 1)} a_i.$$

Subcase R-9-b

Consider Figure 16(b) and define

$$\vartheta = \frac{3r_{j-1/2}+2}{3(2r_{j-1/2}+1)}.$$

Then, by evaluating $f_{i,j}$ and rearranging,

$$b_i = f_{i,j} - \vartheta a_i$$

and

$$f_{i,j+1} = \frac{-(a_i+b_i)}{3a_i(2r_{j-1/2}+3)}\left[(a_i+b_i)\left(\frac{-(a_i+b_i)}{a_i}\right) + 3(r_{j-1/2}+1)(a_i+b_i)\right].$$

Substituting for b_i in the above results in a cubic equation for a_i, i.e.

$$c_0 a_i^3 + c_1 a_i^2 + c_2 a_i + c_3 = 0,$$

where

$$c_0 = (1-\vartheta)^3 - 3(r_{j-1/2}+1)(1-\vartheta)^2,$$

$$c_1 = 3(1-\vartheta)^2 f_{i,j} - 6(r_{j-1/2}+1)(1-\vartheta)f_{i,j} - 3(2r_{j-1/2}+3)f_{i,j+1},$$

$$c_2 = -3f_{i,j}^2(r_{j-1/2}+\vartheta), \qquad c_3 = f_{i,j}^3.$$

Subcase R-9-c

Similarly in Figure 16(c),

$$\vartheta = \frac{9r_{j-1/2}+14}{3(2r_{j-1/2}+3)}, \qquad \zeta = 1-\vartheta,$$

$$b_i = f_{i,j+1} - \vartheta a_i,$$

$$c_0 a_i^3 + c_1 a_i^2 + c_2 a_i + c_3 = 0,$$

$$c_0 = \zeta^2(3r_{j-1/2}+3-\zeta),$$

$$c_1 = \zeta[3(r_{j-1/2}+1)(f_{i,j+1}+1) - 2\zeta f_{i,j+1} - \zeta] - \zeta(1-f_{i,j+1})[3(r_{j-1/2}+1) - \zeta] - 3(2r_{j-1/2}+1)f_{i,j} + 3(1-\zeta)^2 + 6r_{j-1/2}(1-\zeta),$$

$$c_2 = 6(1-\zeta)(1-f_{i,j+1}) + (1-f_{i,j+1})[6r_{j-1/2} - 3(r_{j-1/2}+1)(f_{i,j+1}+1) + 2\zeta f_{i,j+1} + \zeta] + \zeta(2-f_{i,j+1}-f_{i,j+1}^2),$$

$$c_3 = (1-f_{i,j+1})(2-f_{i,j+1}-f_{i,j+1}^2) + 3(1-f_{i,j+1}^2).$$

Subcase R-9-d

For this subcase, two coupled non-linear equations are solved numerically by the Newton–Raphson method. The parameters are defined in Figure 16(d):

$$\varphi(a_i,\ b_i) = (a_i+b_i)^3 - 3(r_{j-1/2}+1)(a_i+b_i)^2 a_i - 3(2r_{j-1/2}+3)f_{i,j} - b_i a_i^2 = 0,$$

$$\psi(a_i, b_i) = (a_i + b_i - 1)[(2a_i + 2b_i + 1)(a_i + b_i - 1) + 3(r_{j-1/2}a_i - b_i + 1)(a_i + b_i + 1)] + 3(1 - b_i)^2 + 6r_{j-1/2}a_i(1 - b_i) - 3(2r_{j-1/2} + 1)f_{i,j}a_i^2 = 0.$$

As for the axial direction, closed form solutions for a_i and b_i do not exist and the case needs to be distinguished by trial and error.

II.2. Interface advection in the radial direction

The interface advection in the radial direction as described in Section 5 requires determination of the interface line $\eta = \mathscr{G}(\xi), \xi_e$ and the volume function $V(\xi)$. Once these functions are known, the volume flux can be calculated from equation (25). Therefore in the following the governing equations for calculating the volume flux for the basic cases are given. Cases I-a–I-d are for downward advection; cases II-a–II-d are for upward advection.

Subcase I-b

In this subcase the interface is reconstructed by a line segment connecting the left cell face to the right cell face in a single wet cell as shown in Figure 8. The equations for η, ξ_e and $V(\xi)$ are

$$\eta = l + \frac{1 - \xi}{\theta},$$

$$\xi_e = 1 - \theta(\eta_e - l),$$

$$V(\xi) = \frac{\pi\xi}{3}\left[\left(r_{j-1/2} + l + \frac{1}{\theta}\right)^2 + \left(r_{j-1/2} + l + \frac{1}{\theta}\right)\left(r_{j-1/2} + l + \frac{1 - \xi}{\eta}\right) + \left(r_{j-1/2} + l + \frac{1 - \xi}{\theta}\right)^2 - 3r_{j-1/2}^2\right],$$

where $\theta = \tan\bar{\theta}$.

Subcase I-c

$$\eta = \frac{1 - l - \xi}{\theta},$$

$$\xi_e = 1 - l - \theta\eta_e,$$

$$V(\xi) = \begin{cases} \pi(2r_{j-1/2} + 1)\xi & \text{if } \xi \leqslant 1 - l - \theta, \\ \pi(2r_{j-1/2} + 1)(1 - l - \theta) + \dfrac{\pi(\xi + l + \theta - 1)}{3}\left[(r_{j-1/2} + 1)^2 + (r_{j-1/2} + 1)\left(r_{j-1/2} + \dfrac{1 - l - \xi}{\theta}\right) + \left(r_{j-1/2} + \dfrac{1 - l - \xi}{\theta}\right)^2 - 3r_{j-1/2}^2\right] \\ \qquad \text{if } 1 - l - \theta < \xi < l. \end{cases}$$

Subcase I-d

$$\eta = \frac{1}{\theta}(l - \xi),$$

$$\xi_e = l - \theta\eta_e,$$

$$V(\xi) = \frac{\pi\xi}{3}\left[\left(r_{j-1/2} + \frac{l}{\theta}\right)^2 + \left(r_{j-1/2} + \frac{l}{\theta}\right)\left(r_{j-1/2} + \frac{l-\xi}{\theta}\right) + \left(r_{j-1/2} + \frac{l-\xi}{\theta}\right)^2 - 3r_{j-1/2}^2\right].$$

Subcase II-a

For the upward movement of a wet cell, equating the differential volumes results in

$$\eta_e = r_{j+1/2} - \sqrt{(r_{j+1/2}^2 - 2r_{j+1/2}\varepsilon_r)}.$$

The following relations are derived for subcases II-a–II-d shown in Figure 8. Subcases IV-a–IV-d can be reduced to these. For subcase II-a,

$$\eta = \left(1 - \frac{l}{\theta}\right) + \frac{1-\xi}{\theta}, \qquad \xi \geqslant 1 - l,$$

$$\xi_e = 1 - \theta(\eta_e + l\theta - 1),$$

$$V(\xi) = \begin{cases} \pi(2r_{j+1/2} + 1)\xi \quad \text{if } \xi \leqslant 1 - l, \\ \dfrac{\pi(\xi + l - 1)}{3}\left[3r_{j+1/2}^2 - (r_{j+1/2} - 1)^2 - (r_{j+1/2} - 1)\left(r_{j+1/2} - 1 + \dfrac{\xi + l - 1}{\theta}\right)\right. \\ \qquad \left. - \left(r_{j+1/2} - 1 + \dfrac{\xi + l - 1}{\theta}\right)^2\right]. \end{cases}$$

Subcase II-b

$$\eta = l + \frac{1-\xi}{\theta},$$

$$\xi_e = 1 - \theta(\eta_e - l),$$

$$V(\xi) = \frac{\pi\xi}{3}\left[\left(r_{j-1/2} + l + \frac{1}{\theta}\right)^2 + \left(r_{j-1/2} + l + \frac{1}{\theta}\right)\left(r_{j-1/2} + l + \frac{1-\xi}{\eta}\right) + \left(r_{j-1/2} + l + \frac{1-\xi}{\theta}\right)^2 - 3r_{j+1/2}^2\right].$$

Subcase II-c

$$\eta = \frac{1 - l - \xi}{\theta},$$

$$\xi_e = 1 - l - \theta\eta_e,$$

$$V(\xi)=\begin{cases}\pi(2r_{j+1/2}-1)\xi & \text{if } \xi \leqslant 1-l-\theta,\\ \pi(2r_{j+1/2}-1)\xi+\dfrac{\pi(\xi+l+\theta-1)}{3}\left[(r_{j+1/2}-1)\left(r_{j+1/2}-1+\dfrac{\xi+l+\theta-1}{\theta}\right)\right.\\ \quad\left.+\left(r_{j+1/2}-1+\dfrac{\xi+l+\theta-1}{\theta}\right)^2-2(r_{j+1/2}-1)^2\right] & \text{if } 1-l-\theta<\xi<l.\end{cases}$$

Subcase II-d

$$\eta=\frac{1}{\theta}(l-\xi),$$

$$\xi_e=l-\theta\eta_e,$$

$$V(\xi)=\frac{\pi\xi}{3}\left[3r_{j+1/2}^2-\left(r_{j+1/2}-\frac{l}{\theta}\right)^2-\left(r_{j+1/2}-\frac{l}{\theta}\right)\left(r_{j+1/2}-\frac{l-\xi}{\theta}\right)\right.$$
$$\left.-\left(r_{j+1/2}-\frac{l-\xi}{\theta}\right)^2\right].$$

REFERENCES

1. J. M. Hyman, 'Numerical methods for tracking interfaces', *Physica D*, **12**, 396–407.
2. K. J. Laskey, E. S. Oran and J. P. Boris, 'Approaches to resolving and tracking interfaces and discontinuities', *Naval Research Laboratory Report 5999*, Arlington, VA, 1987.
3. J. M. Floryan and H. Rasmussen, *Appl. Mech. Rev.*, **42**, 323–341 (1989).
4. R. B. DeBar, 'Fundamentals of the KRAKEN code', *Lawrence Livermore Laboratory Report UCID-17366*, 1974.
5. W. F. Noh and P. Woodward, 'SLIC (simple line interface calculation)', in A. I. van de Vooren and P. J. Zandbergen (eds), *Lecture Notes in Physics*, Vol. 59, *Proc. Fifth Int. Conf. on Numerical Methods in Fluid Dynamics*, NY, 1976, pp. 330–340.
6. A. J. Chorin, 'Flame advection and propagation algorithm', *J. Comput. Phys.*, **95**, 1 (1980).
7. A. J. Chorin, 'Curvature and solidification', *J. Comput. Phys.*, **57**, 472 (1985).
8. A. F. Ghoniem, A. J. Chorin and A. K. Oppenheim, 'Numerical modeling of turbulent combustion in premixed gases', *Proc. Eighteenth Symp. (Int.) on Combustion*, Combustion Institute, Pittsburgh, PA, 1981, pp. 1375–1383.
9. A. F. Ghoniem, D. Y. Chen and A. K. Oppenheim, 'Formation and inflammation of a turbulent jet', *AIAA J.*, **24**, 224–229 (1986).
10. J. A. Sethian, 'Curvature and the evolution of fronts', *Commun. Math. Phys.*, **101**, 487 (1985).
11. P. Colella, L. F. Henderson and E. G. Puckett, 'A numerical study of shock wave refractions at a gas interface', *Proceedings of the AIAA 9th Computational Fluid Dynamics Conference*, Buffalo, New York, 1989, pp. 426–439.
12. L. F. Henderson, P. Colella and E. G. Puckett, 'On the refraction of shock waves at a slow-fast gas interface', *J. Fluid Mech.*, **224**, 1 (1991).
13. E. G. Puckett, 'A numerical study of shock wave refraction at a CO_2/CH_4 interface', in J. Glimm and A. J. Majda (eds), *The IMA Volumes in Mathematics and Its Applications*, 29, *Multidimensional Hyperbolic Problems and Computations*, Springer, New York, 1991, p. 261.
14. C. W. Hirt and B. D. Nichols, 'Volume of fluid (VOF) method for the dynamics of free boundaries', *J. Comput. Phys.*, **39**, 201 (1981).
15. B. D. Nichols, C. W. Hirt and R. S. Hotchkiss, 'SOLA-VOF: a solution algorithm for transient fluid flow with multiple free boundaries', *Los Alamos Scientific Laboratory Report LA8355*, 1980.
16. J. D. Ramshaw and J. A. Trapp, 'A numerical technique for low-speed homogeneous two-phase flow with sharp interfaces', *J. Comput. Phys.*, **21**, 438–453 (1976).
17. K. H. Hain, 'The partial donor cell method', *J. Comput. Phys.*, **73**, 131–147 (1987).
18. P. K. Barr and W. T. Ashurst, 'An interface scheme for turbulent flame propagation', *Sandia National Laboratory Report SAND82-8773*, 1984.
19. D. L. Youngs, 'Time-dependent multi-material flow with large fluid distortion', K. W. Morton and M. J. Baines (eds), *Numerical Methods for Fluid Dynamics*, Academic, New York, 1982, p. 27.
20. D. L. Marcus, E. G. Puckett, J. B. Bell and J. S. Saltzman, 'Numerical simulation of accelerated interfaces', in *Proc. Third Int. Workshop on the Physics of Compressible Turbulent Mixing*, Abbey of Rayaumont, June 1991.